Properties of Mg-Al alloys in relation to hydrogen storage

Andreasen, A.

Publication date:
2005

Document Version
Publisher's PDF, also known as Version of record

RISØ

Risø-R-1523(EN)

Properties of Mg-Al alloys in relation to hydrogen storage

Anders Andreasen

Materials Research Department

Risø National Laboratory
Roskilde
Denmark
August 2005

Author: Anders Andreasen
Title: Properties of Mg-Al alloys in relation to hydrogen storage
Department: Materials Research Department

Abstract: Magnesium theoretically stores 7.6 wt. % hydrogen, although it requires heating to above 300 degrees C in order to release hydrogen. This limits its use for mobile application. However, due to its low price and abundance magnesium should still be considered as a potential candidate for hydrogen storage e.g. in stationary applications. In this report the properties of Mg-Al alloys are reviewed in relation to solid state hydrogen storage Alloying with Al reduces the hydrogen capacity since Al does not form a hydride under conventional hydriding conditions, however both the thermodynamical properties (lower desorption temperature), and kinetics of hydrogenation/dehydrogenation are improved. In addition to this, the low price of the hydride is retained along with improved heat transfer properties and improved resistance towards oxygen contamination.

Risø-R-1523(EN)
August 2005

ISSN 0106-2840
ISBN 87-550-3459-4

Contract no.:

Group's own reg. no.: 1625049-00

Sponsorship:

Cover :

Pages: 22
Figures: 10
Tables: 6
References: 92

Risø National Laboratory
Information Service Department
P.O.Box 49
DK-4000 Roskilde
Denmark
Telephone +45 46774004
bibl@risoe.dk
Fax +45 46774013
www.risoe.dk

Contents

1 Introduction

Hydrogen storage in magnesium has been the subject of an intense research effort during the last 30 years, mainly due to its high theoretical gravimetric hydrogen density of $\rho_m(H_2) = 7.6$ wt.%. However, due to slow kinetics and a high thermodynamic stability of MgH_2, heating to above 300 °C is required in order to release hydrogen. This is the ultimate show stopper for the usage of magnesium as a hydrogen storage medium in combination with a PEM fuel cell in future mobile applications.

A variety of alloying elements have been explored in order to bring down the hydrogen desorption temperature, although with limited success. Mg_2Ni being one of the most successful attempts still require more than 250 °C in order to release hydrogen at 1 bar. Thus, hydrogen storage applications based on magnesium seems to be limited to either traditional combustion engines or fuel cells working at higher temperatures than the PEM.

Besides the high gravimetric hydrogen capacity one of the great advantages of magnesium compared to traditional hydrides such as the AB (e.g. TiFe), AB_2 (e.g. $TiCr_2$) and AB_5 (e.g. $LaNi_5$, $CaNi_5$) mainly being based in transition metals and rare earth elements, is its abundance and its price. Magnesium is the 8. most abundant element in the earths crust and one cubic meter of seawater contains 1.3 kg Mg. The price of Mg is approx. 3 $/kg in comparison with a price of 4-15 $/kg for Ni, Ti, V and Cr and a price of 350 $/kg for La. Thus, in terms of price pr. stored kg of H_2 is superior to most traditional hydrides.

In this report the hydrogen storage properties of Mg-Al are reviewed. When alloying with Al the low price is retained (Al price approx. 1.3 $/kg) and Al adds improved heat transfer to the hydride bed, which is essential for fast dehydrogenation. In addition to this it is generally found that the thermodynamics and kinetics of Mg-Al compared to Mg are improved along with the resistance towards oxygen contamination. The focus of this review will be hydrogen capacity, thermodynamics of hydride formation, kinetics of hydrogenation/dehydrogenation, oxidation behaviour in relation to the kinetics of hydrogenation/dehydrogenation and finally the reaction mechanism of dehydrogenation.

2 Phase diagram and stable alloy phases

The phase diagram of Mg-Al includes at least four stable phases [1, 2]: the fcc solid solution of magnesium in aluminum, the hcp solid solution of aluminum in magnesium, the β-phase (Mg_2Al_3) and the γ-phase ($Mg_{17}Al_{12}$). Furthermore, a line compound *R* also denoted ϵ at approx. 56-58 at.% aluminum is known to exist [1, 2]. Several metastable and high-temperature phases have been proposed e.g. γ', $MgAl_2$, λ, λ' [1, 2, 3, 4].

Phase	Composition range [at.% Mg]	Sg.	Lattice parameters [Å]
(Al)	0-18.6	$Fm\bar{3}m$	a = 4.05-4.22
β(Mg_2Al_3)	38.5-40.3	$Fd\bar{3}m$	a = 28.22-28.16
R	42	R3	a = 12.82
			c = 21.75
γ($Mg_{17}Al_{12}$	45-60.5	$I\bar{4}3m$	a = 10.47-10.61
(Mg)	89-100	$P6_3/mmc$	a = 3.16-3.20
			c = 5.16-5.21

Table 1: Mg-Al phases. Information extracted from ref. [3, 1, 4].

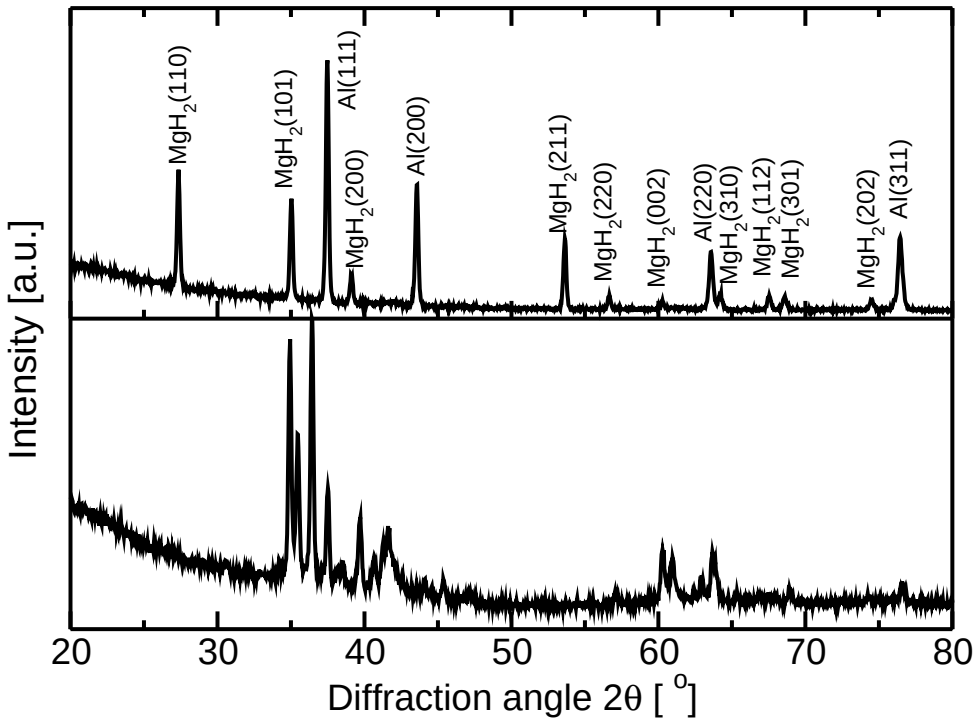

Figure 1: X-ray diffraction patterns of an Mg-Al alloy in the hydrogenated state (top) and dehydrogenated state (bottom). Data are from ref. [11].

3 Hydrogenation/dehydrogenation behaviour

Only few studies on the hydrogenation/dehydrogenation behaviour of Mg-Al alloys (ranging from solid solution of Al to true alloys) have been reported [5, 6, 7, 8, 9, 10, 11]. It is generally observed that upon hydrogenation the Mg-Al alloy disproportionates under formation of MgH_2 and Al according to the sceme below

$$\mathrm{Mg_xAl_y + xH_2 \rightarrow xMgH_2 + yAl} \tag{1}$$

during dehydrogenation Mg and Al reacts and an Mg-Al is recovered. This is illustreted in Figure 1. In the dehydrogenated state only MgH_2 and Al is present, after dehydrogenation diffraction peaks from MgH_2 and Al are absent and only those corrosponding an Mg-Al alloy (mainly β-phase) are present. Some authors find that due to incomplete hydrogenation the reaction product, in addition to MgH_2 and Al, also contains a small amount of an Mg-Al alloy with lower Mg content than the host alloy [8, 9].

The reason for the disproportionation of Mg-Al alloys during hydrogenation may be explained by a relatively high thermodynamic stabillity of MgH_2 compared to that of the alloy [6, 12] combined with a relatively low stabillity of a Mg-Al-H compound [13, 14]. Formation of AlH_3 will not occur during hydrogenation of Mg-Al since the temperature applied to reach acceptable kinetics for MgH_2 exceeds the decomposition temperature of AlH_3 ($\Delta H = -30$ kJ/mol H_2, $T_{dec} \approx 150\,^{\circ}$C) unless a very high hydrogen pressure is applied [15, 16]. Magnesium alanate ($Mg(AlH_4)_2$), belonging to the class of so-called complex hydrides, have recently received a great deal of attention due to its high hydrogen density [17, 18, 19]. Although the dehydrogenation product is an Mg-Al alloy [18, 20] reversiblity viz. formation of $Mg(AlH_4)_2$ from an Mg-Al alloy have only been observed using severe reaction conditions under a hydrogen plasma [10].

Phase	Mg concentration [at.%]	x	y	$\rho_m(H_2)$ [wt.%]
(Mg)	89-100	0.89-1	0.11-0	6.87–7.66
γ($Mg_{17}Al_{12}$	58.6	17	12	4.44
R	42	42	58	3.17
β(Mg_2Al_3)	40	2	3	3.02

Table 2: Mg-Al phases and their theoretical gravimetric hydrogen density calculated with Eq. 2.

The theoretical gravimetric hydrogen storage capacity, $\rho_m(H_2)$, of Mg-Al alloys can be easily estimated from reaction eq. 1 in wt.% as

$$\rho_m(H_2) = \frac{xM_{H_2}}{xM_{H_2} + xM_{Mg} + yM_{Al}} 100 \quad (2)$$

where M_{H_2}, M_{Mg}, and M_{Al} are the molar mass of hydrogen, magnesium and aluminum, respectively. Table 2 summarizes calculated storage capacities of the stable Mg-Al phases (excluding Al(Mg) solid solution).

4 Oxidation and surface segregation

4.1 Effect of surface oxide on the hydrogenation kinetics of Mg

It is known that hydrogen diffusion in the close packed MgO is extremely poor [21] and strongly thermally activated compared to diffusion of hydrogen in Mg [22] and MgH_2[23]. The presence of an oxide layer/shell on magnesium particles therefore lowers the rate of MgH_2 formation/decomposition [24]. In fact Hjort *et al.* [25] have shown that the rate of hydrogen uptake at room temperature in Pd-coated Mg films decreased 2 orders of magnitude when exposed to oxygen in an UHV system equipped with a high pressure cell. Further, exposing the sample to air at ambient conditions lead to a decrease in the uptake rate of 3 orders of magnitude. Pedersen *et al.* [26, 27] have investigated the effect of cycling magnesium powder in impure hydrogen. They found that introducing impure hydrogen containing approx. 5000 ppm O_2 lead to a decrease in hydrogen uptake capacity due to a decreased uptake rate compared to that in hydrogen with less than 1 ppm total impurities. Furthermore, activation of air exposed Mg by at least 1 cycle of hydrogenation/dehydrogenation is necessary in order to obtain steady-state kinetics [28]. The applied activation procedure covers different phenomena including penetration of the surface oxide film, followed by hydrogenation leading to cracking of particles (including oxide film), due to the crystal lattice expansion associated with the hydride formation and the brittle nature of the hydride [29, 30, 31, 5].

We have previously compiled representative values of the apparent activation energy of dehydrogenation for magnesium samples with different compositions, investigated with different methods and subject to different activation procedures [24]. The general picture found was, that E_A for dehydrogenation of activated samples lies in the range 100-170 kJ/mol, while E_A for non-activated samples is significantly higher and close to 300 kJ/mol. This may be rationalized in terms of creation of an MgO film on Mg particles as discussed previously.

4.2 Oxidation of the pure metals

The oxidation behavior of Mg is well investigated. A 1-2 nm thick oxide layer builds up within minutes when Mg is exposed to air. This MgO layer reaches approx. 3 nm after 2 hours and

continues to grow slowly following a logarithmic growth rate and the oxide thickness reaches approx. 4-5 nm within 10 months [32, 33, 34, 28, 35]. Both temperature and moisture can increase the speed of oxide growth [34].

The initial oxidation of Al during exposure to water vapour is quite similar to Mg although the logarithmic growth rate is somewhat lower. During extended periods of exposure under ambient conditions the oxide growth on Al seems to terminate with an oxide thickness of approx. 2 nm [32, 33].

4.3 Oxidation and surface segregation of Mg-Al alloys

Palasantzas et. al. [36] have studied the electron beam induced oxidation of Mg-Al alloys under UHV conditions (base pressure $\sim 4 \cdot 10^{-8}$ Pa) and . The main oxidants being H_2O and CO from the UHV atmosphere. They showed that, in general, the oxidation of Mg_2Al_3 was promoted by the electron beam yielding an oxide thickness of approx. 6-7 nm whereas unexposed areas (oxidation due to oxygen chemisorption only) of both Mg_2Al_3 and (Al) reached an oxide thickness of only 2 nm. Electron beam oxidation of the Al(Mg) solid solution resulted in mainly Al being oxidized. For Mg_2Al_3 both Al and Mg were oxidized accompanied by Mg surface segregation under oxide formation. No surface segregation was found for the Al(Mg) solid solution in agreement with ref. [37]. However, at temperatures above 300 °C Mg surface segregation have been shown to exceed that in Mg_2Al_3 [37].

Using XPS McIntyre and Chen [35] have investigated oxide formation on Mg alloys with Al content from 3-8.5 at.% exposed under ambient conditions. They showed that the Mg-Al alloys initially develop oxide films with a thickness of approx. 3.5 nm compared to pure Mg which develops a film with a thickness of 3 nm. However, the subsequent oxide film growth rate for the Mg-Al alloys is much lower than for pure Mg - both reaching an oxide film thickness of 4 nm after 7 days of exposure.

Scotto-Sheriff et al. [38] have investigated the composition and structure of the oxide film on Aluminum alloys with 4-5 at.% Mg. They found an oxide film thickness of approx. 4 nm consisting of MgO and Al_2O_3 in a 1:1 ratio due to Mg surface segregation. Electron diffraction suggests that both oxides are present in an amorphous state. Annealing at 360 °C leads to increased surface segregation of Mg (as MgO which remains amorpheous) and partly crystallization of Al_2O_3. It is also found that metallic Al is present in the outer most layer of the surface, propably due to reduction of Al_2O_3 by Mg.

Using XPS and AES Shamir et al. [39] have studied the oxidation behaviour of $Mg_{0.95}Al_{0.05}$ and $Mg_{0.55}Al_{0.45}$. They found that for air-exposed samples surface Mg was present in an oxidized state mainly while Al was present in both metallic and oxidized state in agreement with the observations of Scotto-Sheriff et al. as outlined above. It was also observed that significant surface segregation of magnesium had taken place both in the air-exposed sample and after combined sputtering/oxygen exposure.

From the above we can summarize some general trends in the oxidation behaviour of Mg-Al alloys. Since both Mg and Al have a strong affinity towards oxide formation ($\Delta H_{MgO} = 1200$ kJ/mol O and $\Delta H_{Al_2O_3} = 1116$ kJ/mol O) alloying does apparently not prevent surface oxidation. Due to a lower surface energy the transport of Mg atoms to the surface is energetically favourable. Combined with a higher oxygen affinity, surface segregation of Mg is promoted by air-exposure. The significance of the oxidation behaviour of Mg-Al alloys in relation to e.g. hydrogen uptake is not exactly unambiguous, although there are some indications of somewhat improved properties compared to pure Mg: 1) The presence of both surface MgO, Al_2O_3 and possibly metallic Al, might enhance the formation of a less compact oxide layer as also proposed for surface segregated Mg_2Ni and Mg_2Cu [40, 41]. 2) A lower oxide growth rate for alloyed samples compared to pure Mg might suggest a higher resistance towards deactivation

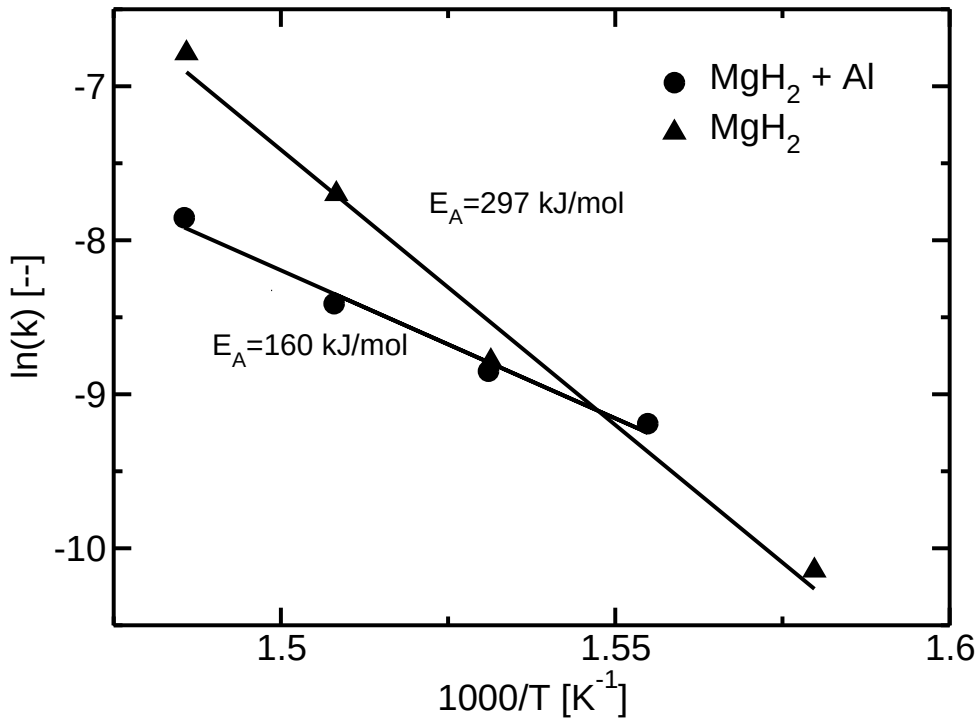

Figure 2: Arrhenius plots of dehydrogenation rate constants for air-exposed Mg and air-exposed Mg-Al. Data are from ref. [43, 11].

during continued cycling in the presence of impurities. 3) The presence of a partly amorphous oxide layer even at elevated temperatures may offer favorable hydrogen diffusion paths [29, 42].

Some evidence for the positive effect of alloying on the sensitivity towards surface contamination can be found in recent results on air-exposed and non-activated samples of pure MgH_2 [43] and MgH_2 + Al (obtained from hydriding of $Mg_{17}Al_{12}$) [11]. The results are summarized in the form of Arrhenius plots of experimentally determined dehydrogenation rate constants in figure 2. As seen from the figure the apparent activation energy (equal to the slope in an Arrhenius plot) for dehydrogenation of Mg is high due to oxygen contamination as discussed previously. Interestingly, the apparent activation energy for dehydrogenation of the aluminum containing sample is comparable to that of activated Mg. Similar results have been obtained for MgH_2/Mg_2Cu and $MgH_2/MgCu_2$ [44].

5 Thermodynamics

5.1 Alloy formation

Miedema and co-workers have proposed a semi-empirical model known as the *Miedema model* for the formation enthalpy of transition metal alloys and metallic alloys between transition metals and non-transition metals. The basis of the model is the Wigner-Seitz concept of atomic cells [45, 46, 47]. The model was originally developed for alloying between metal atoms but have also been extended to account for binary, ternary, and quaternary metal hydride heats of formation [48, 49, 50, 51, 52].

In the following we will estimate the heat of formation of Mg-Al alloys using the *Miedema* model.

$$\Delta H_{alloy} = \frac{2f(c^s)(c_A V_A^{2/3} + c_B V_B^{2/3})}{(n_{ws}^A)^{-1/3} + (n_{ws}^B)^{-1/3}} \times \left[-P(\Delta\Phi^*)^2 + Q(\Delta n_{ws}^{1/3})^2\right] \quad (3)$$

where c_A and c_B are atomic concentrations of elements A and B, V_A and V_B are the molar volumes, $\Delta\Phi^* = \Phi_A^* - \Phi_B^*$ is the difference in electronegativity, $\Delta n_{ws}^{1/3} = (n_{ws}^A)^{-1/3} - (n_{ws}^B)^{-1/3}$, where n_{ws}^A and n_{ws}^B are the electron densities of A and B at the boundary of their Wigner-Seitz cells, respectively, Q and P are constants, and $f(c^s)$ is a function of the atomic concentrations given by:

$$f(c^s) = c_A^s c_B^s \left[1 + 8(c_A^s c_B^s)^2\right] \quad (4)$$

with

$$c_A^s = \frac{c_A V_A^{2/3}}{c_A V_A^{2/3} + c_B V_B^{2/3}} \quad (5)$$

$$c_B^s = \frac{c_B V_B^{2/3}}{c_A V_A^{2/3} + c_B V_B^{2/3}} \quad (6)$$

Equations 3 through 6 is used to calculate the formation enthalpy of Mg-Al alloys as a function of composition with parameters for magnesium and aluminum given in table 3. The result is shown in figure 3. Comparison is also made with previously reported values.

	Φ^*	$n_{ws}^{1/3}$	$V^{2/3}$	P	Q/P
	[V]	[(d.u.)$^{1/3}$]	[cm^2]		[eV^2/(d.u.)$^{2/3}$]
Mg	3.45	1.17	5.8		
				10.6	9.4
Al	4.20	1.39	4.6		

Table 3: Parameters used in the calculation of the heat of formation of mg-al alloys by the *Miedema* model. Parameters are from ref. [46, 47]

5.2 Hydride formation

In order to experimentally evaluate hydride formation enthalpies usually Pressure-Composition-Isotherms are invoked. Corresponding plateau pressures (the pressure related to the two phase region viz. co-excistance of metal/intermetallic and metal hydride) and temperatures are related through the Van't Hoff equation [5, 29, 53, 54, 55]

$$\ln\left(\frac{p_{H_2}}{p^\ominus}\right) = \frac{\Delta H^\ominus}{RT} - \frac{\Delta S^\ominus}{R} \quad (7)$$

where $\Delta H^\ominus$ and $\Delta S^\ominus$ are the change in standard enthalpy and the change in standard entropy, respectively, from now on denoted ΔH_f and ΔS_f. According to the Van't Hoff equation the enthalpy and entropy of hydride formation are determined from a Van't Hoff plot of $\ln(p_{H_2}/p^\ominus)$ vs. reciprocal temperature as the slope and intercept, respectively . Hence, from a number of measurements of plateau pressures at different temperatures the Van't Hoff equation can by applied to determine ΔH_f and ΔS_f. Usually ΔS_f is around -130 J/(mol K) which roughly corresponds to the H_2 molecule loosing its translational degrees of freedom upon transformation from the gas phase into the solid state of the hydride.

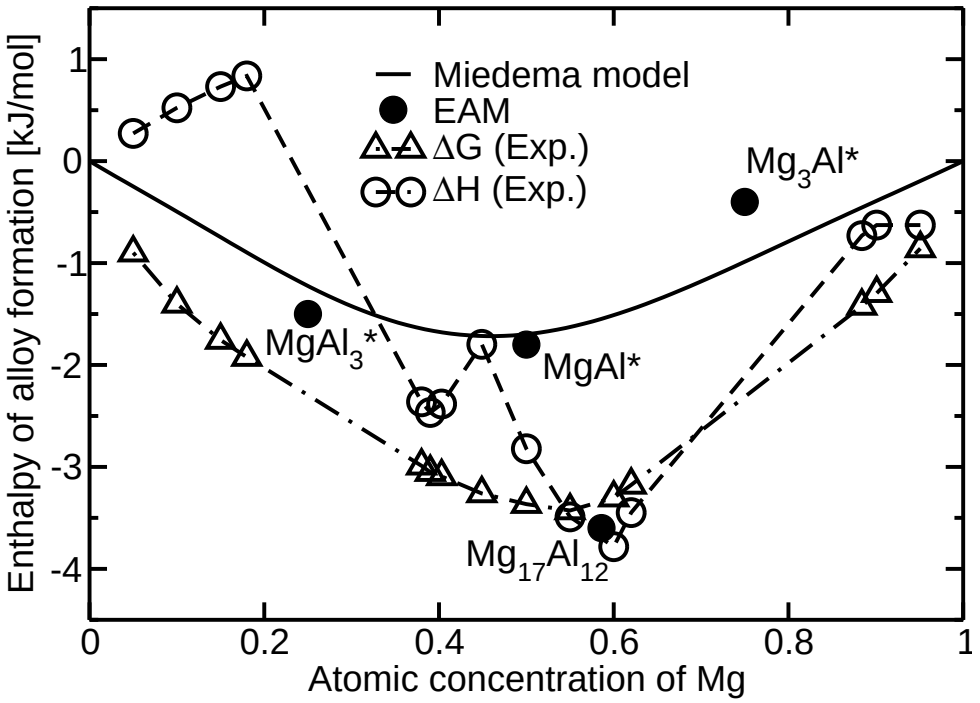

Figure 3: Predicted alloy formation enthalpy for Mg-Al alloys as a function of composition using the Miedema model. Included for comparison is also theoretical values from Embedded Atom Model (EAM) calculations from ref. [12]. Alloys marked with an asterisk is either hypothetical or metastable.

Only a few plateau pressures of Mg-Al alloys have been reported [5, 6, 7]. The reported plateau pressures have been used to construct a Van't Hoff plot in figure 4. For comparison a Van't Hoff plot is also included for pure Mg obtained by fitting ΔH_f and ΔS_f in Eq. 7 to the comprehensive compilation of experimentally determined plateau pressures published by Zeng et al. [56]. In addition, a plot (designated Miedema) based on ΔH_f for the hydrogenation on Mg-Al is included as calculated by the following equation

$$\Delta H_f = \Delta H_f(MgH_2) + \frac{1}{x}\Delta H_{alloy} \tag{8}$$

based on the decomposition of reaction Eq. 1 into the following two reactions

$$\mathrm{Mg_xAl_y} \rightarrow \mathrm{xMg + yAl} \tag{9}$$

$$\mathrm{xMg + xH_2} \rightarrow \mathrm{xMgH_2} \tag{10}$$

where x is chosen as the composition of the Mg-Al alloy giving the maximum heat of formation as indicated by figure 3 and ΔH_{alloy} is calculated by the Miedema model. $\Delta H_f(MgH_2)$ is taken as the formation enthalpy of pure MgH_2 as found from the data of Zeng et al. ΔS_f used for the Miedema Van't Hoff plot is assumed equal to that of the experimentally determined value for MgH_2. ΔH_f and ΔS_f for the Mg-Al alloy and the values fitted for pure MgH_2 as represented in the Van't Hoff plot are listed in table 4 along with values for a few other Mg based alloys for hydrogen storage.

As seen from figure 4 alloying of Mg with Al generally leads to higher plateau pressures i.e. a lower temperature is required to obtain an equilibrium pressure of 1 bar H_2 (which is the minimum goal for practical applications) than for pure MgH_2. The destabilization of MgH_2 is realized

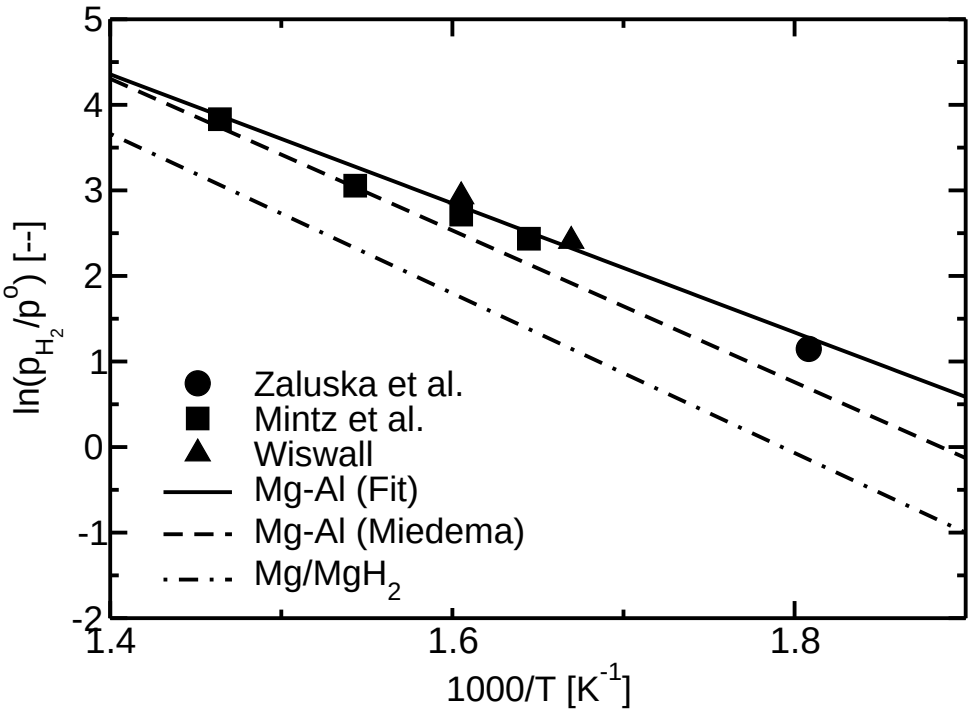

Figure 4: Van't Hoff plot Mg-Al from experiments of Zaluska et al. for γ-phase (circle) [7], Wiswall for β-phase (triangles) [5], and Mintz et al. also for β-phase (squares) [6] including the Van't Hoff fit (full line). Miedema model calculations (dashed line). Data for pure Mg (dash-dotted line) included for comparison [56].

Alloy system	ΔH [kJ/mol]	ΔS [J/(mol K)]	T_{dec} [°C]
Mg-Al-H	-62.7	-124	234
MgH_2	-77.5	-139	284
Mg_2NiH_4	-64.5	-122	255
Mg_2FeH_6	-79.2	-137	305

Table 4: Hydride formation enthalpies and entropies and corresponding decomposition temperatures for different magnesium based hydrogen storage systems. Values for Mg-Ni and Mg-Fe are from ref. [57, 58, 59] and values for Mg are from ref. [56].

	A [s^{-1}]	E_A [kJ/mol]
Adsorption	2.6·10^6	110
Desorption	6.0·10^{12}	106

Table 5: Classical prefactor and activation energies for hydrogen adsorption and desorption, respectively, on Mg(0001) from ref. [22].

due to the exothermic formation of Mg-Al during the endothermic dehydrogenation of MgH_2 + Al resulting in an overall reduction in the heat requirement to desorb H_2. As also observed from figure 4 the Miedema model seems to under-predict the alloy formation enthalpy, ΔH_{alloy} and thus the plateau pressure. However, on an absolute scale the model is successful. From table 4 it is found that the hydride formation enthalpy for Mg-Al alloys are improved compared to both pure Mg, Mg_2FeH_6, and even Mg_2Ni, which is quite interesting since Mg_2Ni is usually viewed as the optimal destabilization of Mg in relation to hydrogen storage applications . Listed in table 4 are also temperatures required to obtain an equilibrium pressure of 1 bar H_2 estimated by rearranging Eq. 7

$$T_{dec} = \frac{\Delta H_f}{\Delta S_f} \tag{11}$$

From the listed T_{dec} it is observed that the decomposition temperature of MgH_2 + Al is lowered approx. 50 °C compared to pure Mg and it is even 20 °C lower than for Mg_2Ni. Although, the thermodynamic parameters for Mg-Al are somewhat uncertain (the standard error of the Van't Hoff fit is 4 kJ/mol), and should preferably be verified by additional measurements of the plateau pressure at different temperatures, in order to draw more solid conclusions. In therms of thermodynamics the hydrogenation behaviour of Mg-Al alloys is apparently quite similar to those of Mg_2Cu which also disproportionates during hydrogenation [5, 41, 60, 61].

6 Hydrogen dissociation

It is generally agreed that magnesium does not promote dissociation of hydrogen molecules, H_2 [62]. Sprunger and Plummer [62, 63] found that exposing both clean Mg(0001) and Mg(11$\bar{2}$0) at 100-150 K to RT H_2 did not result in any detectable hydrogen adsorption. As a consequence, in order to adsorb H-atoms on Mg surfaces, the H_2 is pre-dissociated e.g. over a hot filament [62, 64]. Interestingly, Mintz et al. [65] found that exposing Mg to 2000 L H_2 did not result in any detectable hydrogen dissociation, whereas exposing MgO to the same dose actually lead to hydrogen dissociation with a sticking probability of $8 \cdot 10^{-4}$. Recent, calculation efforts have also been devoted to the study of H_2 dissociation on MgO [66].

Nørskov et al. [67] have calculated the potential energy surface (PES) using a jellium based model for hydrogen dissociation on Mg(0001). These calculations suggested an activation barrier for H_2 dissociation of approx. 50 kJ/mol in qualitative agreement with experiments [63] suggesting that Mg is indeed an activated process. DFT-LDA calculations have shown the bridge site to be energetically favoured for H_2 dissociation with a barrier of approx. 40 kJ/mol [68]. Recent and more accurate DFT-GGA calculations estimate the activation energy for dissociation of hydrogen on Mg(0001) to approx. 100 kJ/mol [22]. In addition to the activation barrier of dissociation also the recombination barrier. Table 5 summarizes the result from ref. [22].

Using the values for adsorption in table 5 we can estimate the initial (in the limit of zero H-coverage) sticking coefficient, σ° for H_2 on Mg(0001) using the following equation

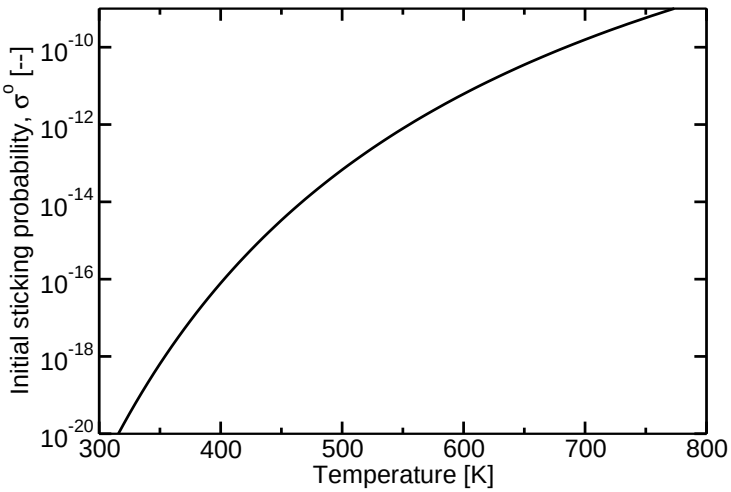

Figure 5: Initial sticking coefficient/probability of H_2 on Mg(0001) calculated at p_{H_2} = 30 bar.

$$\sigma^\circ = \frac{r_f \rho_{site}}{F} \tag{12}$$

with r_f being the forward rate of hydrogen adsorption (neglecting desorption in the limit of zero coverage given by

$$r_f = k_f \frac{p_{H_2}}{p^\ominus} = A \exp\left(-\frac{E_A}{RT}\right) \frac{p_{H_2}}{p^\ominus} \tag{13}$$

and F being the flux of hydrogen molecules given by

$$F = \frac{p_{H_2}}{\sqrt{2\pi m_{H_2} k_B T}} \tag{14}$$

In equation 12 ρ_{site} is the adsorption site density on Mg(0001) calculated from ref. [22]. k_f, p_{H_2}, and $p^\ominus$ in equation 13 are the adsorption rate constant, the hydrogen pressure, and the thermodynamic reference pressure, respectively. m_{H_2} and k_B in equation 14 are the hydrogen molecular mass in a.m.u. and Boltzmans constant, respectively. Figure 5 shows calculated initial sticking coefficient for Mg(0001). The figure is a very clear illustration of the fact that Mg is very poor at dissociating hydrogen e.g. at RT only 1 out of 10^{20} molecules will be dissociated. Even with a flux of hydrogen molecules of 10^{10} this leads to a rate of adsorption being effectively zero. The dissociation probability is strongly enhanced by increasing the temperature, although still at 300 °C it must be considered as very low corresponding to a rate of 0.01 hydrogen molecules being dissociated pr. site every second.

The dissociation ability of Al surfaces are quite similar to those of Mg surfaces. Several papers report that exposing Al surfaces to molecular hydrogen does not result in any dissociation [69, 70, 71]. Paul [69] found that hydrogen desorbs from Al(100) around a temperature of approx. $T_m = 340$ K when heated at a rate of $\beta = 1.3$ K. Assuming a 2. order desorption process and a desorption prefactor of $1 \cdot 10^{13}$ s^{-1} the desorption barrier, E_{des} can be estimated iteratively with the 2. order Redhead equation [72]

$$E_{des} = RT_m \ln\left(\frac{RT_m^2}{E_{des}\beta 2\theta}\right) \tag{15}$$

to approx. 90 kJ/mol which is slightly lower than for Mg(0001). This is in qualitative agreement the experiments of Berger and Rendulic [73] and also with recent DFT-GGA calculations

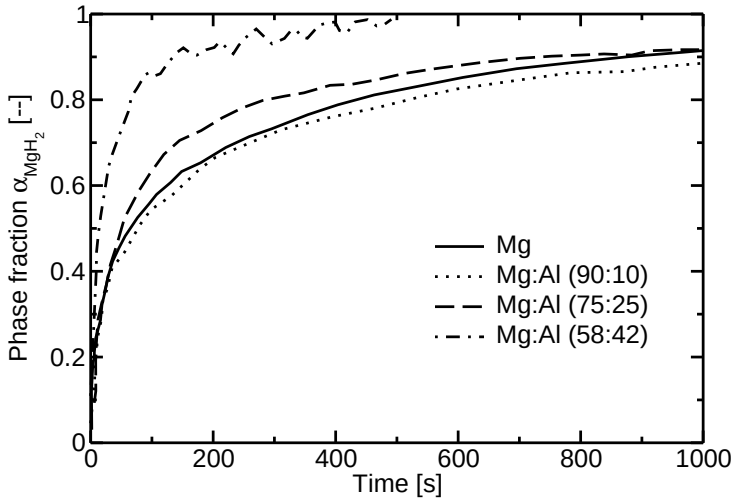

Figure 6: Hydrogenation kinetics of pure un-milled Mg compared with Mg-Al compounds with varying Al content ball milled for 20 h. Hydrogenation performed at T = 400 °C and a hydrogen pressure of 38 bar. Data extracted from ref. [8].

of the activation barrier on Al(110) performed by Hammer et al. [74] which suggests an activation barrier of approx. 50 kJ/mol for dissociative adsorption.

It is actually quite difficult to judge to which degree the presence of Al in Mg-Al improves the ability to dissociatively adsorb hydrogen compared to pure Mg. First of all, no precise measurements of the sticking probabilities for H_2 on either Mg or Al have been reported. Second, the physical properties of the Mg-Al may be different from those of the pure hosts. Although, the similarities in dissociation behaviour between Mg and Al, and the presence of a sizable barrier for both adsorption and desorption on both systems may indicate that potential improvements are negligible. Instead, in order to promote the dissociation, addition of Ni have proven to be effective [7, 75, 76, 77] even in small amounts, due to the negligible activation barrier for hydrogen dissociation [78, 79, 80, 81] for this metal.

7 Hydrogenation/dehydrogenation kinetics

Relatively few studies on the kinetics of hydrogenation and dehydrogenation of Mg-Al alloy particles have been reported. Mintz et al. [82] studied the effect of dilute group IIIA element (Al, Ga, and In) additions on the apparent activation energy of hydrogenation of Mg. It was observed that small amounts of Al ($<$2 at.%) in Mg lead to a decrease in apparent activation energy, whereas for higher concentrations of Al (4 at. %) the apparent activation energy approached that of pure Mg [82]. According to Mintz et al. this suggests improvements to be diffusion related.

Bouaricha et al. [8] have studied the effect of higher Al concentrations on the hydrogenation kinetics of Mg-Al alloys. Their results are shown in figure 6. As seen in the figure the hydrogenation behaviour of un-milled Mg and ball milled $Mg_{90}Al_{10}$ are more or less identical. Thus apparently no improvements of the kinetics have been achieved at a 10 at.% concentration of Al, which is in agreement with the findings of Mintz et al. [82] for higher Al concentrations as discussed above. However, after leaching (selective removal of Al, hydrogenation curve not shown) the rate constant of hydrogenation was more than doubled compared to pure Mg. Bouaricha et al. [8] concluded that this was in agreement with the observations of lower ap-

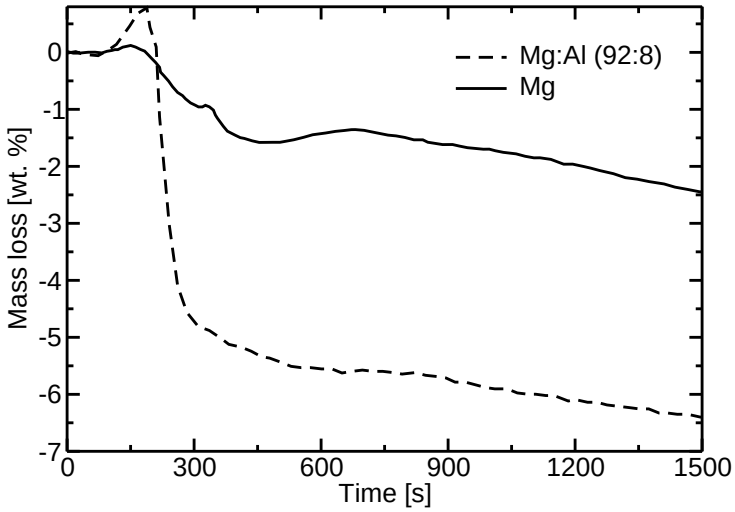

Figure 7: Dehydrogenation kinetics of pure Mg and Mg:Al (92:8) ball milled for 20 h obtained by heating from RT at t = 100 s to T = 300 °C at t = 400 s. From t = 400 s the temperature is maintained at approx. 300 °C. Data extracted from ref. [13].

parent activation energies as discussed above. However, during leaching, the surface area increased by a factor of 2.2. Thus, the higher rate constant for the lower Al contents might just as well be explained by a change in prefactor.

According to figure 6 it is evident that higher concentrations of Al leads to significantly improved hydrogenation kinetics, especially for the sample with a composition corresponding to that of the γ-phase ($Mg_{17}Al_{12}$). The same effect is observed for the dehydrogenation kinetics. Shang et al. [13] found that for a low Al concentration of 8 at.% the dehydrogenation kinetics was significantly improved (cf. figure 7) which is in contrast to the findings of Bouaricha et al. [8] for their 10 at.% Al sample.

Since, all samples in figure 6 were well activated prior to the kinetic measurements, the observed effect is likely different than the surface effect related to oxidation behaviour as discussed previously in section 4.3. Instead, it seems more likely to be related to a bulk effect, probably due to improved hydrogen diffusion through Al or in the additional grain boundaries between MgH_2 and Al. Some justification of this hypothesis can be found in the fact that hydrogen diffusivity in Al (at 300 K) is similar to Mg or slightly improved [22, 83, 84] whereas hydrogen diffusion in both Al and Mg is significantly better than for MgH_2 [23]. Further, the formation of a stable surface hydride film blocking hydrogen diffusion [29, 31, 76, 85, 86, 87, 88] is less probable due to the creation of Al grains during hydrogenation of Mg-Al facilitating hydrogen diffusion in analogy with MgH_2/Mg_2Cu [41, 89, 90, 91].

8 Reaction mechanism for dehydrogenation of MgH_2+Al

Recently, Andreasen et al. studied the isothermal dehydrogenation kinetics of MgH_2 + Al (formed by hydrogenation of Mg-Al with approximate stoichiometric ratio of 50:50) at different temperatures applying *in situ* X-ray powder diffraction (XRPD) [11]. A typical result of such *in situ* XRPD studies is shown in figure 8.

At $t = 0$ s the diffraction pattern corresponds to the one shown in figure 1 (upper) i.e. the host alloy has undergone complete disproportionation during hydrogenation. Thus only diffraction peaks corresponding to MgH_2 and Al are present. During heating from RT to the

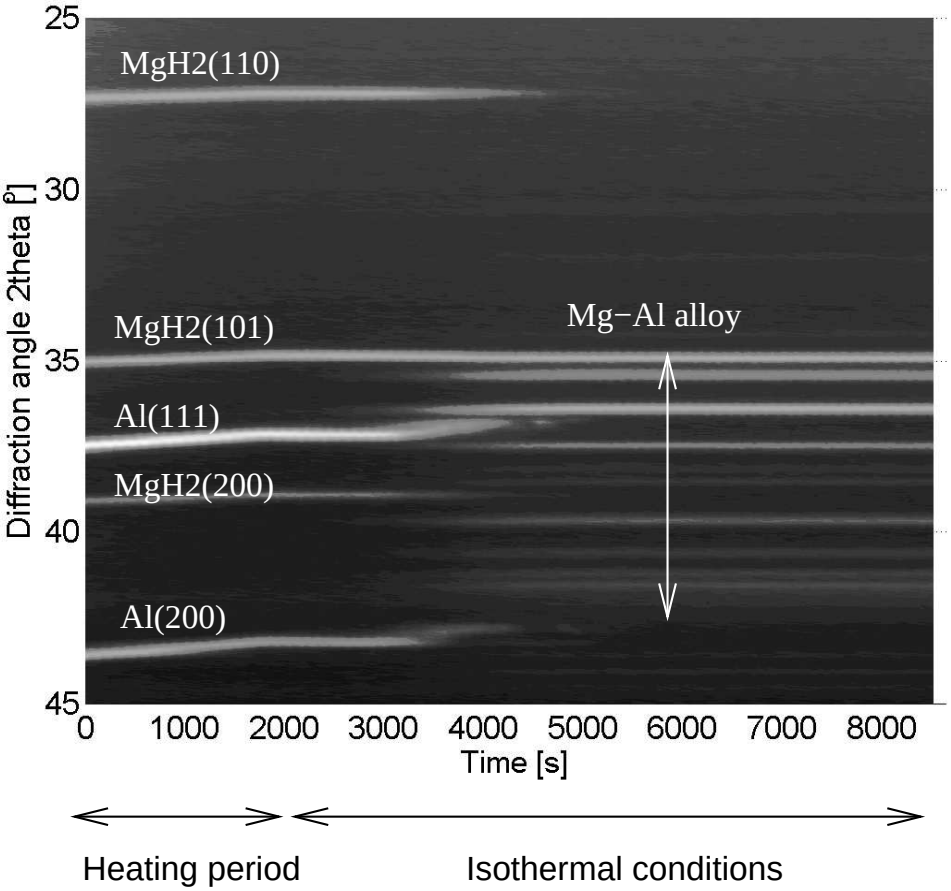

Figure 8: Series of consecutive *in situ* XRPD patterns stacked chronologically from left to right. High intensity corresponds to bright areas and low intensity correspond to dark areas. Figure is from ref. [11]. Isothermal temperature is 400 °C. See ref. [11] for experimental details etc.

α_{MgH_2}	$2\theta_{Al}$	a [Å]	$2\theta_{Al(Mg)}$	a [Å]	$I_{Al(Mg)}/I_{Al}$
1.00	38.14	4.087	37.92	4.110	0.04
0.89	38.15	4.086	37.88	4.114	0.18
0.81	38.12	4.089	37.84	4.118	0.27
0.73	38.07	4.094	37.79	4.123	0.24

Table 6: Fitting parameters from the gaussian fits to the Al(111) reflection at different degrees of dehydrogenation. Included are also calculated lattice parameters. Corresponding diffraction peaks are shown in figure 9.

isothermal temperature (T = 400 °C) corresponding to approx. $t = 0 - 2000$ s all diffraction peaks shift towards lower values of 2θ corresponding to the thermal expansion of the crystal lattices. Although, the thermal expansion coefficient of MgH_2 seems to be lower than for Al. When the isothermal temperature is reached the diffraction peaks remain constant in 2θ. The dehydrogenation of MgH_2 + Al is visualized by the concurrent decrease in intensity of the MgH_2 and the Al peaks and the simultaneous occurrence of diffraction peaks corresponding to those of an Mg-Al alloy.

Diffraction peaks corresponding to pure Mg are not observed at any time during dehydrogenation. This strongly suggest that the dehydrogenation of MgH_2 as outlined below

$$\mathrm{MgH_2} \rightarrow \mathrm{Mg} + \mathrm{H_2} \tag{16}$$

is slow compared to the subsequent removal of pure Mg due to the formation of an Mg-Al alloy. From figure 8 it is evident that at least two types of Mg-Al phases are present during dehydrogenation. First, the formation of an β-phase Mg-Al alloy which remains throughout the dehydrogenation as visualized by the series of diffraction peaks in the range $2\theta = 35 - 45$ °. Second, the down shift in the diffraction angle of the Al peaks at $t = 3000 - 5000$ s, concurrent with the creation of the Mg-Al alloy, clearly suggests that a solid solution of Mg in Al is formed during dehydrogenation [4, 92]. The down shift in diffraction angle is caused by the lattice expansion due to replacement of Al atoms with larger Mg atoms. In contrast to the formed Mg-Al alloy, the Al(Mg) solid solution phase is of intermediate nature, and only exists until MgH_2 have been completely dehydrogenated. Based on the above observations two additional reaction steps can be proposed

$$\mathrm{Mg} + \mathrm{Al} \rightarrow \mathrm{Al(Mg)} \tag{17}$$

$$\mathrm{Mg} + \mathrm{Al(Mg)} \rightarrow \mathrm{Mg_2Al_3}\ (\beta - \mathrm{phase}) \tag{18}$$

assuming that the Mg-Al alloy nucleates and grows from the Al(Mg) solid solution, only, and not from Al. However, from figure 8 it is very difficult to distinguish if the initial alloy formation actually proceeds from pure Mg and Al or from an Al(Mg) solid solution with a low concentration of Mg.

In order to get a more detailed view of the initial formation of Al(Mg) from Al the Al(111) reflection is plotted for different degrees of dehydrogenation (phase fraction, α of MgH_2) in figure 9. In order to get a rough estimate the Al(111) reflection is fitted with two gaussians. It is seen from 9 that even before dehydrogenation the Al(111) can be explained by a minor phase corresponding to a solid solution and a major phase corresponding to pure Al (or at least a lower concentration of Mg as compared with the minor phase). This suggests that some Mg is not hydrogenated which also, at least partially, explains the incomplete hydrogenation often reported [6, 7, 11]. Table 6 summarizes the fitting parameters and it is noticed that during dehydrogenation the amount of Al(Mg) compared to Al increases to a more or less constant

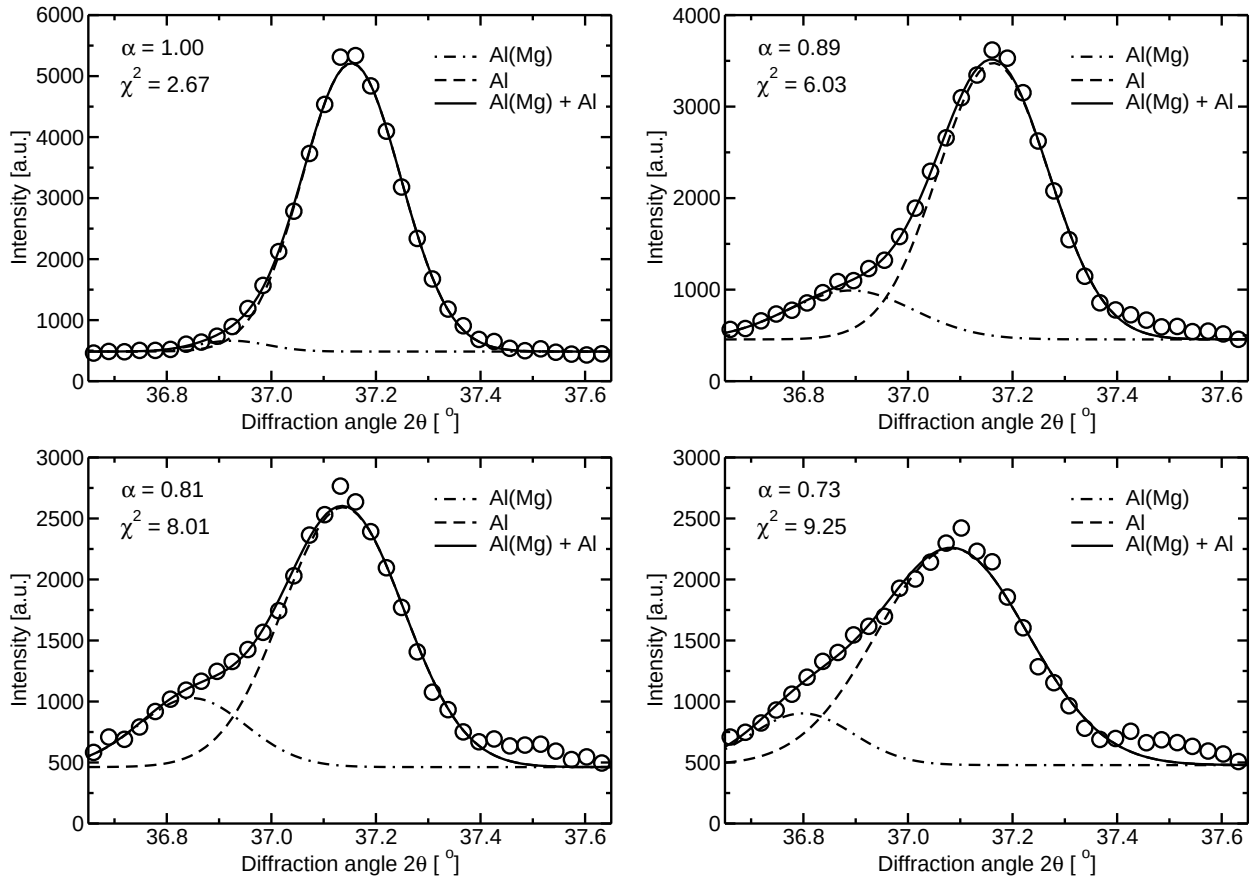

Figure 9: Decomposition of the Al(111) reflection corresponding to different phase fractions of MgH_2 into pure Al and Al(Mg). Isothermal temperature is 400 °C. See ref. [11] for experimental details etc.

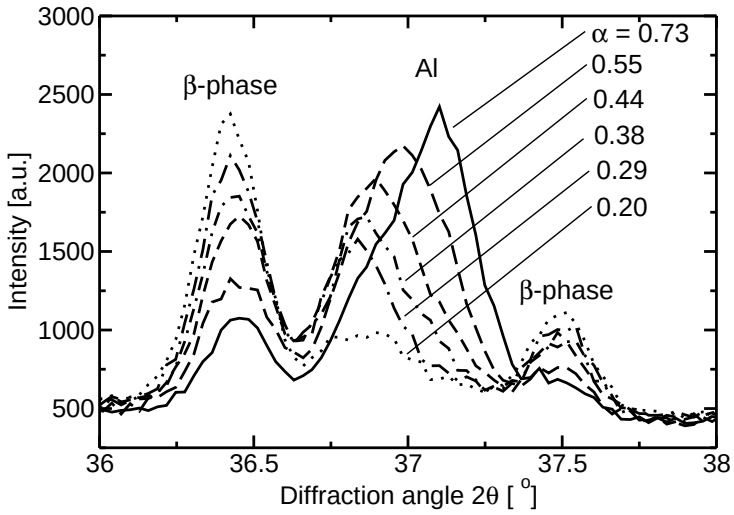

Figure 10: Corresponding diffraction peaks of the (111) reflection of Al(Mg), reflections of β-phase, and phase fractions of MgH_2. Isothermal temperature is 400 °C. See ref. [11] for experimental details etc.

level during the depletion of Al corresponding to phase fractions of MgH_2 from 1-0.73. From the peak positions shown in table 6, the concentration of Mg in Al(Mg) increases as evident from the down shift in 2θ while the position of the Al peak is more or less constant until a phase fraction $<$0.81 is reached. From then also the Al phase is populated with Mg as evident from the continuous down shift in 2θ shown in both figure 8 and figure 10. Using the calculated lattice parameters from table 6 and the relation between lattice Al lattice parameter and magnesium content given in ref. [4] it can be estimated that the Al phase prior to dehydrogenation contains approx. 5 at.% Mg. When the dehydrogenation has started including the formation β-phase, the concentration of Mg in Al(Mg) is approx. 7 at.%, which is quite interesting since the Mg-Al phase diagram suggests that formation of β-phase first takes place when the Mg concentration exceeds approx. 13 at.% [4]. This indicates that the formation of β-phase is somewhat inhomogenous and localized.

9 Summary

The hydrogen storage properties of magnesium can be effectively modified by alloying with aluminum. The main conclusions from this review is listed below.

Capacity. The theoretical hydrogen capacity of pure magnesium of 7.6 wt.% H_2 is effectively lowered when alloying with aluminum due to the fact that hydrogen is bonded as MgH_2. Unless severe reaction conditions are applied Al does not take up hydrogen. The hydrogen content of the three stable Mg-Al phases are 4.44, 3.17, and 3.02 wt.% H_2 for the γ-phase, the R-phase, and the β-phase respectively.

Thermodynamics. Compared to pure magnesium the plateau pressure experienced for Mg-Al alloys are generally higher – which is explained by a reduction (less exothermic) in the enthalpy of hydride formation due to an endothermic disproportionation of the Mg-Al prior to MgH_2 formation. Based on a compilation of available experimentally determined plateau pressures of the Mg-Al-H system the enthalpy of hydride formation is approximated to be

-62.7 kJ/mol H_2 (compared to -77.5 kJ/mol H_2 for pure Mg). This is even lower than the enthalpy of hydride formation of -64.5 kJ/mol H_2 Mg_2Ni.

Kinetics. The literature on hydrogenation/dehydrogenation kinetics of Mg-Al alloys is relatively sparse, although a few studies suggests that Mg-Al alloys have improved kinetics compared to Mg. In their pure state both magnesium and aluminum are poor at dissociating hydrogen thus improvements of the hydrogenation/dehydrogenation kinetics are likely to be associated with other phenomena than hydrogen dissociation/recombination e.g. diffusion.

Oxidation. The apparent activation energy of dehydrogenation of air-exposed MgH_2/Al is 160 kJ/mol compared to almost 300 kJ/mol for air-exposed Mg. This suggest that alloying with Al creates a compound less sensitive towards oxidation probably due to the formation of a less dense oxide layer e.g. amorphous alumina with improved hydrogen diffusion properties compared to close packed MgO.

Acknowledgement

This work has received financial support from the The Danish Technical Research Council through the Center of Excellence *Towards a hydrogen based society* and from

References

[1] T. B. Massalki (Ed.), Binary Alloy Phase Diagrams, Vol. 1, ASM International, 1992.

[2] H. L. Su, M. Harmelin, P. Donnadieu, C. Baetzner, H. J. Seifert, H. L. Lukas, G. Effenberg, F. Aldinger, J. Alloys Comps. 247 (1997) 57–65.

[3] P. Villars (Ed.), Pearson's Handbook Desk Edition, Vol. 2, ASM International, 1997.

[4] J. L. Murray, Bull. Alloy Phase Diagrams 3 (1982) 60–74.

[5] G. Alefeld, J. Völkl (Eds.), Hydrogen in metals II, Vol. 29 of Topics in Applied Physics, Springer-Verlag, 1978.

[6] M. H. Mintz, Z. Gavra, G. Kimmel, J. Less-Common Met. 74 (1980) 263–270.

[7] A. Zaluska, L. Zaluski, J. Ström-Olsen, Appl. Phys. A 72 (2001) 157–165.

[8] S. Bouaricha, J. P. Dodelet, D. Guay, J. Huot, S. Boily, R. Schulz, J. Alloys Comps. 297 (2000) 282–293.

[9] H. Takamura, T. Miyashita, A. Kamegawa, M. Okada, J. Alloys Comps. 356-357 (2003) 804–808.

[10] L. Pranevicius, D. Milcius, L. L. Pranevicius, G. Thomas, J. Alloys Comps. 373 (2004) 9–15.

[11] A. Andreasen, M. B. Sørensen, R. Burkarl, B. Møller, A. M. Molenbroek, A. S. Pedersen, J. W. Andreasen, M. M. Nielsen, T. R. Jensen, J. Alloys Comps. Accepted.

[12] X.-Y. Liu, P. P. Ohotnicky, J. B. Adams, C. Lane Rohrer, R. W. Hyland Jr., Surf. Sci. 373 (1997) 357–370.

[13] C. X. Shang, M. Bououdina, Y. Song, Z. X. Guo, Int. J. Hydrogen Energy 29 (2004) 73–80.

[14] Y. Song, Z. X. Guo, R. Yang, Phys. Rev. B. 69 (2004) 094205.

[15] D. R. Lide (Ed.), Handbook of Chemistry and Physics, 78th Edition, CRC Press LLC, 1997.

[16] G. Sandrock, J. Reilly, J. Graetz, W.-M. Zhou, J. Johson, J. Wegryzn, Appl. Phys. A. 80 (2005) 687–690.

[17] M. Fichtner, O. Fuhr, J. Alloys Comps. 345 (2002) 286–296.

[18] M. Fichtner, O. Fuhr, O. Kircher, J. Alloys Comps. 356–357 (2003) 418–422.

[19] A. Fossdal, H. W. Brinks, M. Fichtner, B. C. Hauback, J. Alloys Comps. 387 (2005) 47–51.

[20] M. Fichtner, J. Engel, O. Fuhr, O. Kircher, O. Rubner, Mater. Sci. Eng. B. 108 (2004) 42–47.

[21] R. Gonzalez, Y. Chen, K. L. Tang, Phys. Rev. B. 26 (8) (1982) 4637–4645.

[22] T. Vegge, Phys. Rev. B. 70 (2004) 035412.

[23] J. Töpler, H. Buchner, H. Säufferer, K. Knorr, W. Prandl, J. Less-Common Met. 88 (1982) 397.

[24] A. Andreasen, T. Vegge, A. S. Pedersen, J. Phys. Chem. B 109 (2005) 3340–3344.

[25] P. Hjort, A. Krozer, B. Kasemo, J. Alloys Comps. 237 (1996) 74–80.

[26] A. S. Pedersen, B. Vigeholm, J. Kjøller, B. Larsen, Int. J. Hydrogen Energy 12 (1987) 765–771.

[27] A. S. Pedersen, B. Larsen, Int. J. Hydrogen Energy 18 (1993) 297–300.

[28] B. Vigeholm, J. Kjøller, B. Larsen, A. S. Pedersen, Int. J. Hydrogen Energy 8(10) (1983) 809–817.

[29] L. Schlapbach (Ed.), Hydrogen in Intermetallic Compounds II, Vol. 67 of Topics in Applied Physics, Springer-Verlag, 1992.

[30] L. Schlapbach, A. Seiler, F. Stucki, H. C. Siegmann, J. Less-Common Met. 73 (1980) 145–160.

[31] B. Vigeholm, K. Jensen, B. Larsen, A. S. Pedersen, J. Less-Common Met. 131 (1987) 133–141.

[32] C. Chen, S. J. Splinter, T. Do, N. S. McIntyre, Surf. Sci. 382 (1997) L652–L657.

[33] T. Do, S. J. Splinter, C. Chen, N. S. McIntyre, Surf. Sci. 387 (1997) 192–198.

[34] V. Fournier, P. Marcus, I. Olejord, Surf. Interface Anal. 34 (2002) 494–497.

[35] C. Chen, N. S. McIntyre, Corrosion Science 40 (1998) 1697–1709.

[36] G. Palazantzas, D. T. L. van Agterveld, J. T. M. De Hosson, Appl. Surf. Sci. 191 (2002) 266–272.

[37] D. T. L. van Agterveld, G. Palazantzas, J. T. M. De Hosson, Appl. Surf. Sci. 152 (1999) 250–258.

[38] S. Scotto-Sheriff, E. Darque-Ceretti, G. Plassart, M. Aucouturier, J. Mater. Sci. 34 (1999) 5081–5088.

[39] N. Shamir, M. H. Mintz, J. Bloch, U. Atzmony, J. Less-Common Met. 92 (1983) 253–263.

[40] A. Seiler, L. Schlapbach, T. von Waldkirch, D. Shaltiel, F. Stucki, J. Less-Common Met. 73 (1980) 193–199.

[41] A. Karty, J. Grunzweig-Genossar, P. Rudman, J. Appl. Phys. 50 (11) (1979) 7200–7209.

[42] A. B. Belonoshko, A. Rosengren, Q. Dong, G. H. C. Leygraf, Phys. Rev. B. 69 (2004) 024302.

[43] T. R. Jensen, A. Andreasen, T. Vegge, J. W. Andreasen, K. Ståhl, F. Besenbacher, A. Molenbroek, M. M. Nielsen, A. S. Pedersen, Int. J. Hydrogen Energy Submitted.

[44] A. Andreasen, M. B. Sørensen, R. Burkarl, B. Møller, A. M. Molenbroek, A. S. Pedersen, T. R. Jensen, Appl. Phys. A Submitted.

[45] A. R. Miedema, J. Less-Common Met. 32 (1973) 117–136.

[46] A. R. Miedema, P. F. de Châtel, F. R. de Boer, Physica 100B (1980) 1–28.

[47] F. R. de Boer, R. Boom, W. C. M. Mattens, A. R. Miedema, A. K. Niessen, Cohesion in metals - transition metal alloys, Vol. 1 of Cohesion and structure, Elsevier Science Publishers B.V., 1988.

[48] P. Bouten, A. R. Miedema, J. Less-Common Met. 71 (1980) 147–160.

[49] K. H. J. Buschow, P. C. P. Bouten, A. R. Miedema, Rep. Prog. Phys. 45 (1982) 937–1039.

[50] A. R. Miedema, K. H. J. Buschow, H. H. Van Mal, J. Less-Common Met. 32 (1973) 117–136.

[51] J. F. Herbst, J. Alloys Comps. 337 (2002) 99–107.

[52] J. F. Herbst, J. Alloys Comps. 368 (2004) 221–228.

[53] L. Schlapbach, A. Züttel, Nature 414 (2001) 353–358.

[54] A. Züttel, Materials Today 9 (2003) 24–33.

[55] A. Züttel, Naturwissenschaften 91 (2004) 157–172.

[56] K. Zeng, T. Klassen, W. Oelerich, R. Bormann, Int. J. Hydrogen Energy 24 (1999) 989–1004.

[57] G. Sandrock, G. Thomas, Appl. Phys. A. 72 (2001) 153–155.

[58] Hydride information center, http://hydpark.ca.sandia.gov.

[59] A. Reiser, B. Bogdanović, K. Schlichte, Int. J. Hydrogen Energy 25 (2000) 425–430.

[60] J. J. Reilly, R. H. Wiswall, Inorg. Chem. 6 (1967) 2220–2223.

[61] P. Selvam, B. Viswanathan, C. S. Swamy, V. Srinizasan, Int. J. Hydrogen Energy 13 (1988) 87–94.

[62] P. T. Sprunger, E. W. Plummer, Surf. Sci. 307-309 (1994) 118–123.

[63] P. T. Sprunger, E. W. Plummer, Chem. Phys. Lett. 187 (1991) 559–564.

[64] C. W. Ostenfeld, J. C. Davies, T. Vegge, I. Chorkendorff, Surf. Sci. Accepted (2005) –.

[65] M. H. Mintz, J. A. Schultz, J. W. Rabalais, Surf. Sci. 146 (1984) 457–466.

[66] A. D'Ercole, C. Pisani, J. Chem. Phys. 111 (1999) 9743–9753.

[67] J. K. Nørskov, A. Houmøller, P. K. Johansson, B. I. Lundquist, Phys. Rev. Lett. 46 (4) (1981) 257–260.

[68] D. M. Bird, L. J. Clarke, C. Payne, I. Stich, Chem. Phys. Lett. 212 (1993) 518–524.

[69] J. Paul, Phys. Rev. B. 37 (1988) 6164–6174.

[70] J. Paul, F. M. Hoffmann, Surf. Sci. 194 (1988) 419–437.

[71] J. M. Mundenar, R. Murphy, E. W. Plummer, Chem. Phys. Lett. 143 (1988) 593–598.

[72] I. Chorkendorff, J. W. Niemantsverdriet, Concepts of modern catalysis and kinetics, Wiley-VCH, 2003.

[73] H. F. Berger, K. D. Rendulic, Surf. Sci. 253 (1991) 325–333.

[74] B. Hammer, K. W. Jacobsen, J. K. Nørskov, Phys. Rev. Lett. 70 (25) (1993) 3971–3974.

[75] E. Ivanov, I. Konstanchuk, A. Stepanov, V. Boldyrev, J. Less-Common Met. 131 (1987) 25–29.

[76] G. Friedlmeier, M. Groll, J. Alloys Comps. 253-254 (1997) 550–555.

[77] P. Tessier, E. Akiba, J. Alloys Comps. 302 (2000) 215–217.

[78] J. Harris, S. Andersson, Phys. Rev. Lett. 55 (1985) 1583–1586.

[79] H. J. Robota, W. Vielhaber, M. C. Lin, J. Segner, G. Ertl, Surf. Sci. 155 (1985) 101–120.

[80] J. Harris, S. Andersson, Appl. Phys. A. 47 (1988) 63–71.

[81] B. Hammer, J. K. Nørskov, Nature 376 (1995) 238–240.

[82] M. H. Mintz, S. Malkiely, Z. Gavra, Z. Hadari, J. Inorg. Nucl. Chem. 40 (1978) 1949–1951.

[83] G. A. Young Jr., J. R. Scully, Acta. Mater. 46 (1998) 6337–6349.

[84] J. Renner, H. J. Grabke, Z. Metalkd. 69 (1978) 639–.

[85] B. Vigeholm, J. Kjøller, B. Larsen, A. Pedersen, J. Less-Common Met. 89 (1983) 135–144.

[86] J. F. Fernandez, C. R. Sanchez, J. Alloys Comps. 340 (2002) 189–198.

[87] H. H. Park, J.-. Y. Lee, J. Less-Common Met. 103 (1984) 181.

[88] J.-. Y. Lee, H. H. Park, J. S. Han, J. Mater. Sci. 21 (1986) 3952–3956.

[89] M. Au, J. Wu, Q. Wang, Int. J. Hydrogen Energy 20 (1995) 141–150.

[90] K. Yamamoto, Y. Tsushio, S. Tanioka, T. Shimizu, T. Morishita, S. Orimo, H. Fujii, J. Alloys Comps. 243 (1996) 144–150.

[91] K. Yamamoto, S. Tanioka, Y. Tsushio, T. Shimizu, T. Morishita, S. Orimo, H. Fujii, J. Alloys Comps. 243 (1996) 144–150.

[92] J. Gubicza, M. Kassem, G. Ribáric, T. Ungár, Mater. Sci. Eng. A. 372 (2004) 115–122.

Mission

To promote an innovative and environmentally sustainable technological development within the areas of energy, industrial technology and bioproduction through research, innovation and advisory services.

Vision

Risø's research **shall extend the boundaries** for the understanding of nature's processes and interactions right down to the molecular nanoscale.

The results obtained shall **set new trends** for the development of sustainable technologies within the fields of energy, industrial technology and biotechnology.

The efforts made **shall benefit** Danish society and lead to the development of new multi-billion industries.